Consistency of MODIS surface bidirectional reflectance distribution function and albedo retrievals: 2. Validation

Yufang Jin, Crystal B. Schaaf, Curtis E. Woodcock, Feng Gao,[1] Xiaowen Li,[1] and Alan H. Strahler

Department of Geography and Center for Remote Sensing, Boston University, Boston, Massachusetts, USA

Wolfgang Lucht

Potsdam-Institut für Klimafolgenforschung, Potsdam, Germany

Shunlin Liang

Department of Geography, University of Maryland, College Park, Maryland, USA

Received 26 July 2002; revised 6 November 2002; accepted 15 January 2003; published 8 March 2003.

[1] The evaluation of the first available satellite-based global albedo product at 1-km resolution is essential for its application in climate studies. We evaluate the accuracy of the Moderate-Resolution Imaging Spectroradiometer (MODIS) albedo product using available field measurements at Surface Radiation Budget Network (SURFRAD) and Cloud and Radiation Testbed–Southern Great Plains (CART/SGP) stations and examine the consistency between the MODIS surface albedos and the Clouds and Earth's Radiant Energy System (CERES) top-of-the-atmosphere albedos as well as historical global albedos from advanced very high resolution radiometer (AVHRR) and Earth Radiation Budget Experiment (ERBE) observations. A comparison with the field measurements shows that the MODIS surface albedo generally meets an absolute accuracy requirement of 0.02 for our study sites during April–September 2001, with the root mean square errors less than 0.018. Larger differences appear in the winter season probably due to the increased heterogeneity of surface reflectivity in the presence of snow. To examine the effect of spatial heterogeneity on the validation of the MODIS albedos using fine resolution field measurements, we derive an intermediate albedo product from four Landsat Enhanced Thematic Mapper Plus (ETM+) images at 30-m spatial resolution as a surrogate for the distributed field measurements. The surface albedo is relatively homogeneous over the study stations in growing seasons, and therefore the validation during April–September is supported. A case study over three SURFRAD stations reveals that the MODIS bidirectional reflectance distribution function model is able to capture the solar zenith angle dependence of surface albedo as shown by the field measurements. We also find that the MODIS surface shortwave albedo is consistent with the contemporary and collocated CERES top-of atmosphere albedos derived directly from broadband observations. The MODIS albedo is also well correlated with historical surface albedos derived from AVHRR and ERBE observations, and a high bias of 0.016 and a low bias of 0.034 compared to those of the latter albedos are reasonable considering the differences in instruments and retrieval algorithms as well as environmental changes. *INDEX TERMS:* 3322 Meteorology and Atmospheric Dynamics: Land/atmosphere interactions; 3359 Meteorology and Atmospheric Dynamics: Radiative processes; 3360 Meteorology and Atmospheric Dynamics: Remote sensing; *KEYWORDS:* MODIS, surface albedo, validation

Citation: Jin, Y., C. B. Schaaf, C. E. Woodstock, F. Gao, X. Li, A. H. Strahler, W. Lucht, and S. Liang, Consistency of MODIS surface bidirectional reflectance distribution function and albedo retrievals: 2. Validation, *J. Geophys. Res.*, *108*(D5), 4159, doi:10.1029/2002JD002804, 2003.

[1]Also at Research Center for Remote Sensing, Beijing Normal University, Beijing, China.

0148-0227/03/2002JD002804$09.00

1. Introduction

[2] As a key land physical parameter controlling the surface radiation energy budget [*Dickinson*, 1995], surface albedo with an absolute accuracy of 0.02–0.05 is required

by climate models at a range of spatial and temporal scales [*Henderson-Sellers and Wilson*, 1983; *Sellers*, 1993]. However, this objective has not yet been satisfied to the extent that, for instance, global surface albedo maps of such accuracy are not routinely provided. A land cover based scheme is currently adopted in most of the land surface model (LSMs) and general circulation models (GCMs) for the parameterization and specification of surface albedo [*Bonan*, 1996; *Sellers et al.*, 1996; *Hansen*, 1983], although a quantified justification for this scheme is yet to be answered due to the limit of high resolution global albedo data sets. On the other hand, natural landscapes are a collection of nested objects in a hierarchical fashion, and various processes control the biophysical characteristics at different spatial scales [*Woodcock and Harward*, 1992; *Collins and Woodcock*, 2000]. Land surface models usually allow a subgrid specification of land cover proportions to account for the heterogeneity of surface properties within a grid [*Dickinson et al.*, 1993; *Bonan*, 1996], while GCMs are generally implemented at very coarse spatial resolutions [*Trenberth*, 1992]. The increasing spatial resolution of modern climate models makes it necessary to examine spatial features of global surface albedo and the effect of spatial scales on the albedo specification. This calls for a spatially explicit global albedo product with high accuracy and high spatial resolution.

[3] In view of this need, surface albedo, including seven spectral and three broadband albedos, is produced as a standard product along with other radiative quantities from observations acquired by the Moderate-Resolution Imaging Spectroradiometer (MODIS) aboard the Terra (EOS AM-1) platform [*Wanner et al.*, 1997; *Lucht et al.*, 2000a; *Schaaf et al.*, 2002]. As a first global albedo product at a 1-km resolution, the MODIS albedo product can be aggregated to subgrid land surface classes and can be routinely updated for use in weather prediction models. It is also very flexible as far as the spectral specification and the illumination conditions are concerned [*Strahler et al.*, 1996; *Wanner et al.*, 1997].

[4] The evaluation of such a satellite-derived albedo product, however, is essential for users, without which subsequent science would be open to questioning. It is usually undertaken by reference to internal diagnostics and independent measurements [*Rodgers*, 2000]. In a companion paper [*Jin et al.*, 2003], the performance of the MODIS BRDF and albedo retrieval algorithm is evaluated based on the product Quality Assurance (QA) fields, analysis of the input data, and intercomparisons with different retrieval algorithms. The main purpose of this study is to validate the operational MODIS albedo product, namely, to assess its accuracy and to examine its consistency with other global albedo products.

[5] Validation is a procedure to assess the uncertainties of the estimated product by comparing it with ground truth [*Justice et al.*, 2000]. Independent field measurements, on the ground or at a tower, as well as measurements from aircraft, are generally presumed to be ground truth and are often taken as the reference for validation. The validation of satellite-derived products, however, is difficult because satellite observations cover larger areas than in situ measurements [*Lucht et al.*, 2000b]. A key problem arising from such different measurement scales is whether a single ground measurement represents the mean value for the pixel at the satellite scale [*Tian et al.*, 2002]. When land surface is heterogeneous, a number of ground samples are needed to capture the spatial variance of the albedo and hence to represent the mean albedo value over the region covering a satellite pixel [*Lucht et al.*, 2000b]. This, however, poses both logistic and practical difficulties for albedo validation. An alternative is to select relatively homogeneous regions for the validation so that the ground measurement matches well the mean albedo at the satellite scale. Surface albedo also depends on the sun and viewing geometry and atmospheric conditions, which requires contemporary ground and satellite observations for the validation. It is thus not surprising that only a limited number of validation exercises for satellite-derived albedos are found in the literature, such as comparisons of ground-based albedometer measurements and AVHRR-based albedos through spatial modeling [*Lucht et al.*, 2000b].

[6] The Surface Radiation Budget Network (SURFRAD) [*Augustine et al.*, 2000] and the Southern Great Plains (SGP) site of the Cloud and Radiation Testbed (CART) [*Stokes and Schwartz*, 1994] were designed to provide accurate and continuous measurements of the surface radiation budget for climate research. Upward and downward radiation measurements are routinely measured at a temporal resolution of 3 minutes, from which the surface albedo can be calculated. The landform and vegetation are relatively homogeneous over an extended region around these stations. Therefore, these stations can provide ground observations to verify the satellite-based albedo retrievals.

[7] This study uses the field measurements acquired from the above mentioned stations in 2001 to quantify the accuracy of the operational MODIS albedos. The simultaneous and collocated top-of-atmosphere (TOA) albedo [*Wielicki et al.*, 1998] derived from Clouds and Earth's Radiant Energy System (CERES), a broadband instrument on board the same Terra Platform [*Wielicki et al.*, 1996], is also used here for a consistency analysis. To examine if the MODIS albedo is consistent with other commonly used historical data sets of global albedo climatology, a comparison is also undertaken with the independent global albedos derived from the Advanced Very High Resolution Radiometer (AVHRR) [*Csiszar and Gutman*, 1999] and the Earth Radiation Budget Experiment (ERBE) radiometer [*Li and Garand*, 1994].

2. MODIS Albedo Retrieval Algorithm

[8] As described in the companion paper [*Jin et al.*, 2003], the MODIS BRDF and albedo algorithm uses a three-parameter semiempirical RossThick-LiSparse-Reciprocal (RTLSR) BRDF model to characterize the anisotropic reflectivity of the land surface [*Wanner et al.*, 1997; *Lucht et al.*, 2000a; *Schaaf et al.*, 2002]. The MODIS atmospheric correction algorithm uses aerosol and water vapor information retrieved from MODIS observations to derive surface reflectance from TOA radiance [*Vermote et al.*, 1997a]. Cloud-free atmospherically-corrected surface reflectances are then accumulated during each 16 day period, from which the BRDF parameters are first retrieved. Seven

spectral albedos are then derived through angular integration of the retrieved BRDF models. Finally a spectral to broadband conversion [*Liang et al.*, 1999] is used to produce three broadband albedos (0.3–0.7 μm, 0.7–5.0 μm, and 0.3–5.0 μm). In addition to a mainstream process (full inversion), a backup magnitude inversion algorithm is used if there are less than seven clear looks or if observations do not fit the BRDF model well during a 16 day period [*Strugnell and Lucht*, 2001]. The snow/ice flag is turned on if the majority of observations are indicated as snow/ice during a 16 day period, and only those observations are used for the BRDF and albedo snow inversion [*Schaaf et al.*, 2002]. Otherwise, only snow-free observations are used for the retrieval.

3. Validation With Field Measurements

3.1. Station Descriptions

[9] As part of the world-wide baseline surface radiation network, the Surface Radiation Budget Network was established by NOAA's Surface Radiation Research Branch [*Augustine et al.*, 2000]. It has been used to validate shortwave radiation budgets derived from the GOES observations [*Pinker et al.*, 1996]. Currently there are six operating stations that cover climatologically diverse regions over the United States [*DeLuisi et al.*, 1999]. Land cover is relatively homogeneous over an extended region at each station. The station in central Pennsylvania is located on Penn State University's Agricultural Research Farm and that in Bondville is located in an agricultural region southwest of Champaign, Illinois. The Goodwin Creek station is located on rural pasture land to the west of Oxford, Mississippi. The Fort Peck station, located on the Fort Peck Tribes Reservation in Montana, is dominated by grasslands. There is only sparse vegetation at the Desert Rock station, northwest of Las Vegas, Nevada. The land surface of Table Mountain station, north of Boulder, Colorado, is sandy, with a mix of exposed rocks, sparse grasses, desert shrubs and small cactus.

[10] The Southern Great Plains radiation testbed, established by DOE's Atmospheric Radiation Measurement (ARM) Program, is located in Southern Kansas and Northern Oklahoma. The main cover types are croplands, grasslands and savannas. The 21 SGP sites are designed to cover an area roughly 350 km on a side (about the size of a grid cell of a general circulation model). The locations of the instruments were chosen so that the measurements reflect conditions over the typical distribution of land uses within the site.

[11] For both networks, total downward and upward solar radiation (0.28–3.0 μm) were measured every 3 minutes by upward-looking pyranometers mounted on a horizontal platform and inverted pyranometers mounted on 10-m meteorological towers, respectively. The 45° effective field of view of the downward-looking pyranometer translates to an area of about 18 m in diameter on the ground. The direct normal and diffuse shortwave fluxes are also measured by Eppley Normal Incidence Pyranometer and a ventilated and shaded Spectrosun pyranometer. The data sets were averaged to a 1/2 hour time step by the CERES ARM Validation Experiment (CAVE) [*Rutan et al.*, 2001]. In addition, estimates of cloud fraction as seen from the upward-pointing pyranometers are given for certain time periods [*Long and Ackerman*, 2000].

3.2. Time Series of Surface Albedo

[12] We derived the surface albedos from the measured downward and upward radiation at local solar noon for each SURFRAD and CART site. For a better comparison with the MODIS clear sky surface albedos, cloud screening was performed using a threshold of 0.2 for the estimated cloud fraction in the CAVE data set. The field albedos under clear conditions were then averaged over all snow-free days or snow days for each 16-day period during 2001, depending on the snow flag embedded in the MODIS albedo QA product. We used an albedo threshold of 0.5 here to identify daily snow conditions due to the lack of snow information in the CAVE data set.

[13] Note that the field albedos correspond to the actual solar illumination with both direct beam and diffuse radiation, while MODIS provides intrinsic surface albedos (black sky albedo for direct beam at local solar noon and white sky albedo for isotropic diffuse radiation). To obtain MODIS-based albedos comparable with the field measurements, we first calculated the ratios of the measured direct and diffuse downwelling radiation to the total downwelling radiation at local solar noon under clear sky conditions, respectively. The MODIS black sky albedo at local solar noon and the white sky albedo were then weighted by the above ratios to obtain so-called MODIS actual albedos.

[14] Figures 1a–1c shows the annual time series of the MODIS-derived actual albedos and the ground observed albedos in the shortwave for the six SURFRAD sites. To better analyze seasonal changes of vegetation, we also plotted the spectral albedos from MODIS for March (081–097), July(193–209), September(257–273), and November(305–321) in the bottom panel as different lines. The ground measured daily local-solar-noon albedos reveal certain day-to-day fluctuations (dashed lines). In the winter season, the distinct high peaks are apparently caused by snow cover whereas some distinct low values are mainly caused by cloud according to the cloud fraction examination. Cloud increases the fraction of downwelling diffuse radiation on the ground due to multiple scattering and hence increases the relative weight of the white sky albedo in actual albedo. On the other hand, the white sky albedo was shown to be lower than black sky albedo when solar zenith angle is greater than around 45° [*Lucht et al.*, 2000a]. Figure 2 shows that the winter solar zenith angle at local solar noon usually exceeds 45° over SURFRAD stations. This explains the lower surface albedo under cloudy sky in winter. An increase in wetness after a rainfall may also reduce the surface albedo values. The temporal sequences of the 16-day clear-sky ground albedo (solid lines) and the MODIS actual albedo are generally smoother than the daily ground values.

[15] For the Table Mountain station and the Desert Rock station, both the satellite observed and field measured albedos in the shortwave are very stable and the MODIS albedos are in very good agreement with the ground albedos for each season (Figure 1a). In Desert Rock, the spectral property of surface albedo is also very stable.

[16] As illustrated in Figure 1b, the MODIS albedo captures the temporal signatures of surface albedo shown

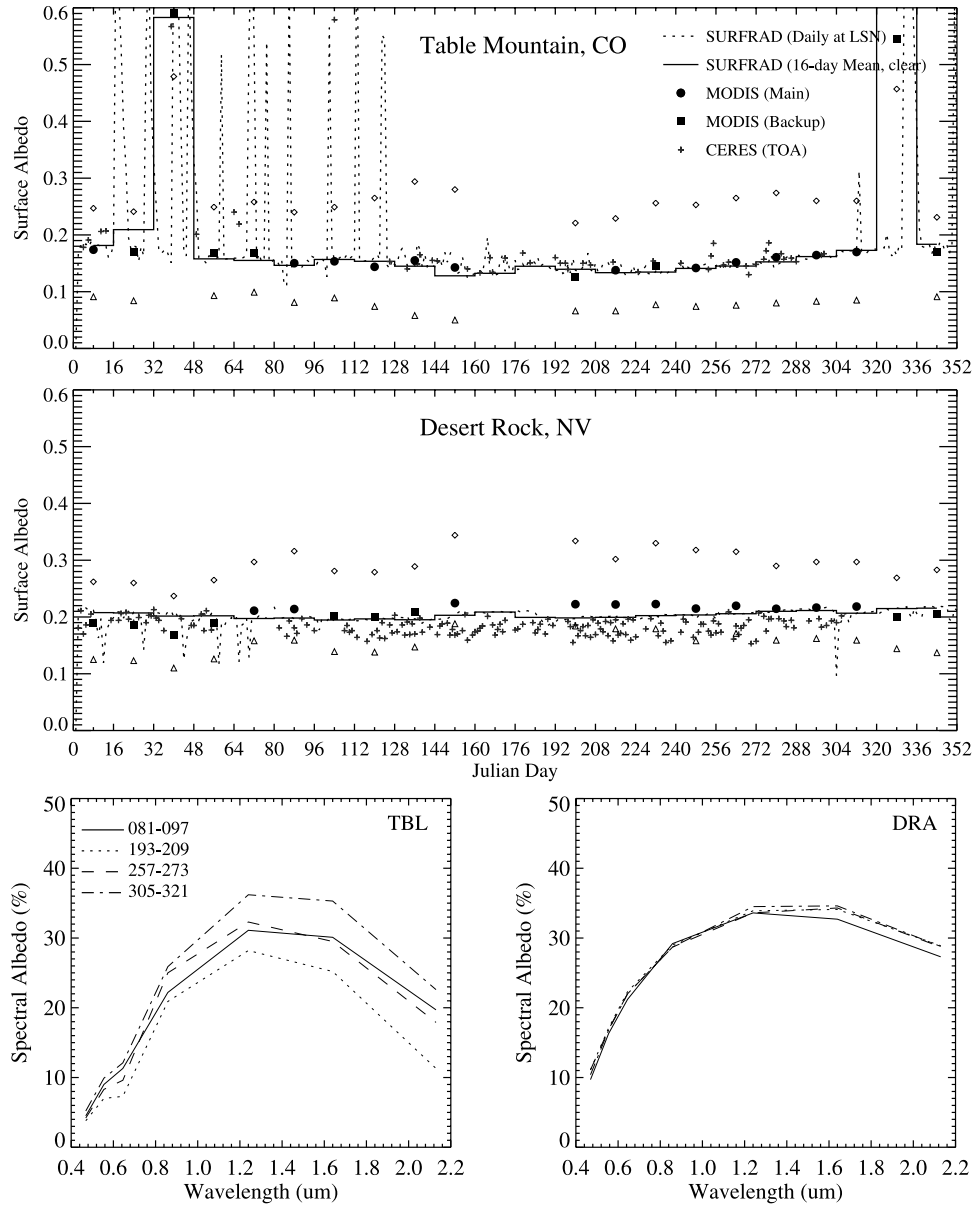

Figure 1a. Temporal sequences of surface shortwave albedos at local solar noon (LSN) as observed from the SURFRAD stations (all sky daily values: dashed line; 16-day averages under clear sky: solid line) and derived from the MODIS operational black sky and white sky albedos for the pixels in which the stations are located. The solid circles and the solid squares represent the MODIS retrievals with the main inversion algorithm and the backup magnitude inversion, respectively. The plus refers to the CERES clear-sky top-of-atmosphere (TOA) albedos averaged over all the footprints within the 15-km radius. The triangle and diamond refer to the MODIS broadband albedos in the visible (VIS) and near infrared (NIR), respectively. The MODIS spectral albedos are shown in the bottom panel for four periods in 2001. Note that the missing data in June is due to the Power Supply 2 shutdown anomaly of the MODIS instrument from 15 June 2001 to 2 July 2001.

in the comparable field measurements, especially in spring, summer, and early fall. In Fort Peck, Montana, both the field and the MODIS surface albedos are above 0.5 in January and February because of snow on the ground. The field data show that the total shortwave albedo decreases slightly from late March and then becomes stable until July. The MODIS shortwave albedo is also rather small and stable during this time period. Moreover, the phenology of vegetation is shown by the increase of the MODIS near-infrared broadband albedo and the decrease of the MODIS visible albedo starting from April when more leaves begin to appear and less bare ground is exposed. Starting from August, the MODIS shortwave albedo increases, similar to the field albedos, as a result of the continuing increase of the visible albedo during vegetation senescence. Similar trends are observed in Goodwin Creek station where pasture land

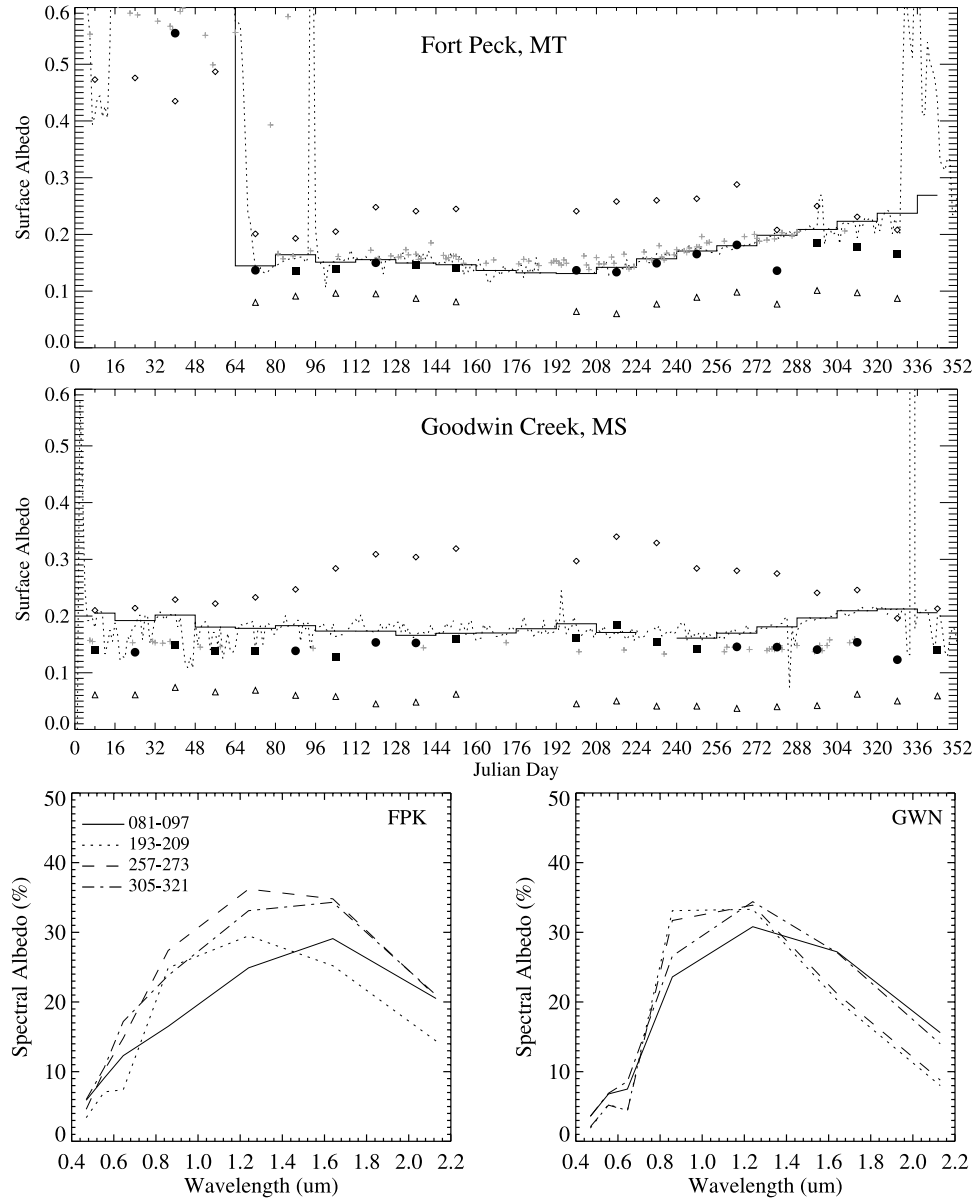

Figure 1b. Same as Figure 1a but for Fort Peck (FPK) and Goodwin Creek (GWN) stations.

is dominant, but the MODIS albedo is lower than the field measurements except in summer. It should also be noted that the solar zenith angle at local solar noon changes from around 20° in summer to around 60° in winter as shown in Figure 2, which also contributes to the annual cycle of surface albedo.

[17] The temporal signatures of the field measurements are more apparent in the Penn State University station and the Bondville station, such as the decrease of shortwave albedos during January–March (Figure 1c). Both stations are located in agricultural areas. The MODIS albedos from both the full inversion and magnitude inversion algorithms agree well with the field measurements during April–September. However, they are lower than the field values by up to 0.05 for the Penn State station and by up to 0.10 for the Bondville station during the winter season. In the shortwave, the MODIS albedo is lower in winter than in summer, which is contrary to the trend as shown in the field measurement. The temporal trend of the MODIS spectral albedos, however, follows the phenology of crops. We found an apparent increase from March to July and a gradual decrease of the near-infrared albedo from July to November. The MODIS albedos in the visible are slightly higher in March and November than those in summer. One possibility for the discrepancy between MODIS and field shortwave albedos is that the in situ field observations may not be representative of the overall MODIS pixel as the ground area seen from a pyranometer is significantly smaller. This scale effect is particularly important when there is extensive landscape heterogeneity. Over agricultural areas, the surface radiative properties are probably more heterogeneous in early spring, late fall and winter, due to snow fall and snow melting as well as rapid vegetation change, than in growing seasons. This issue will be further investigated in the following section.

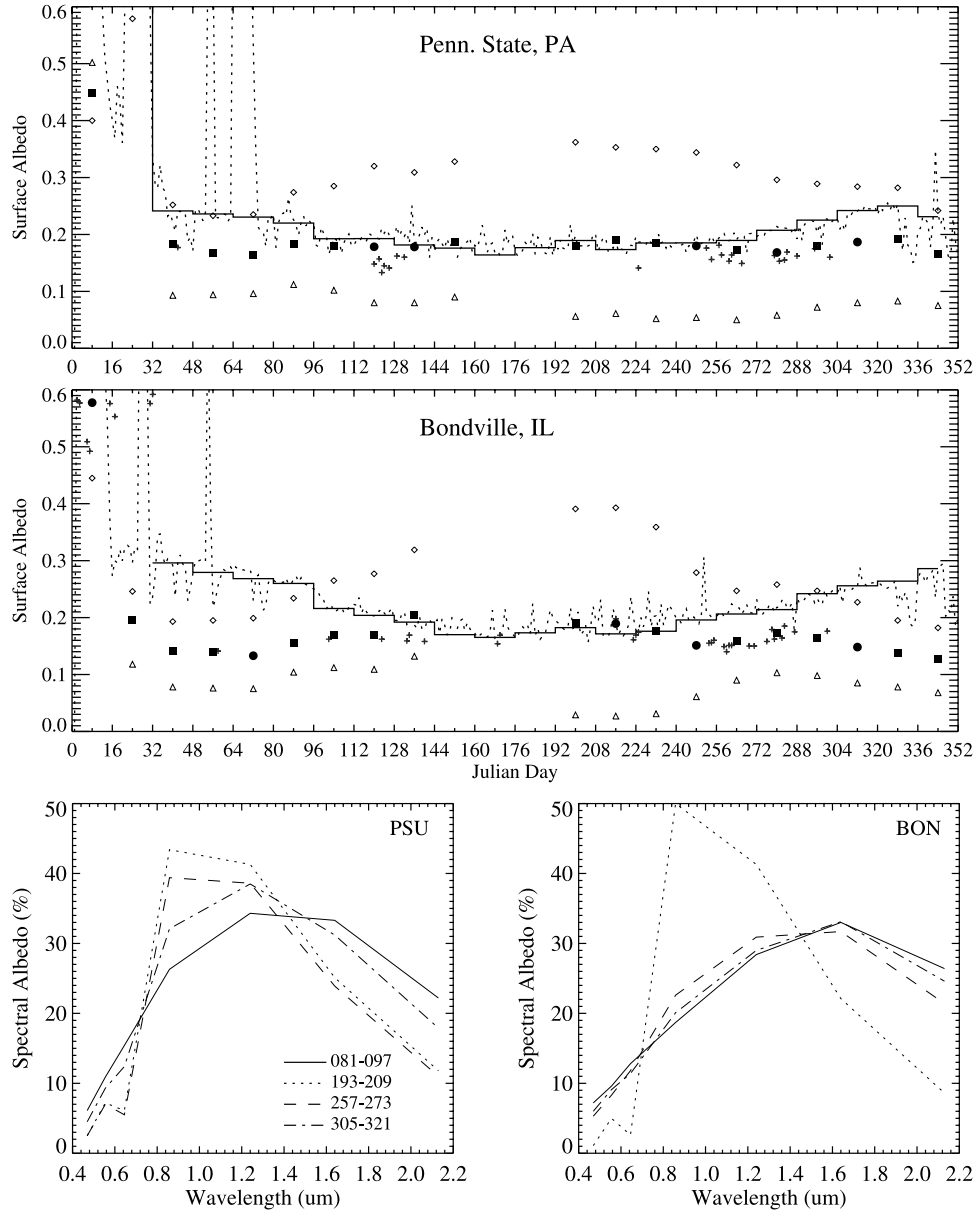

Figure 1c. Same as Figure 1a but for Penn State (PSU) and Bondville (BON) stations.

[18] To exclude the above mentioned possible scale effects of snow cover, snow melting, and vegetation change, Figure 3 plots only the albedos acquired during April–September 2001 for both SURFRAD and CART sites. During these growing seasons, a very good agreement is shown between the MODIS albedos and the field albedos. For the SURFRAD stations, the RMSE is 0.018 and the MODIS albedo has a slightly low bias of 0.004. A RMSE of 0.015 and a lower bias of 0.005 were found for the CART/SGP sites. It is obvious that the MODIS albedo products in green seasons generally meet the absolute albedo accuracy within 0.02 required by climate models, especially over grasslands and croplands. Further studies are needed to investigate the accuracy of MODIS albedo products for large solar zenith angle, where the anisotropy of the downwelling diffuse radiation reduces the accuracy of using the weighted sum of MODIS black sky and white sky albedo to represent surface albedo under actual illumination conditions [*Lewis and Barnsley*, 1994].

3.3. Scale Effects on Surface Albedo Validation

[19] The larger difference between the MODIS albedo and the field values in winter, late fall, and early spring than those in growing seasons suggests the possible effect of spatial heterogeneity within the MODIS pixels on the comparison. Large number of well-sampled ground observations are required to capture the variance of albedos within a larger region where the land reflectivity is heterogeneous. In this case statistics can be derived to validate the MODIS albedo product. However, this method is impractical to implement. Landsat ETM+ observations, with a 30-m spatial resolution, are more comparable with the flux measurements at the tower, and thus can be used as a surrogate for distributed field measurements to examine if

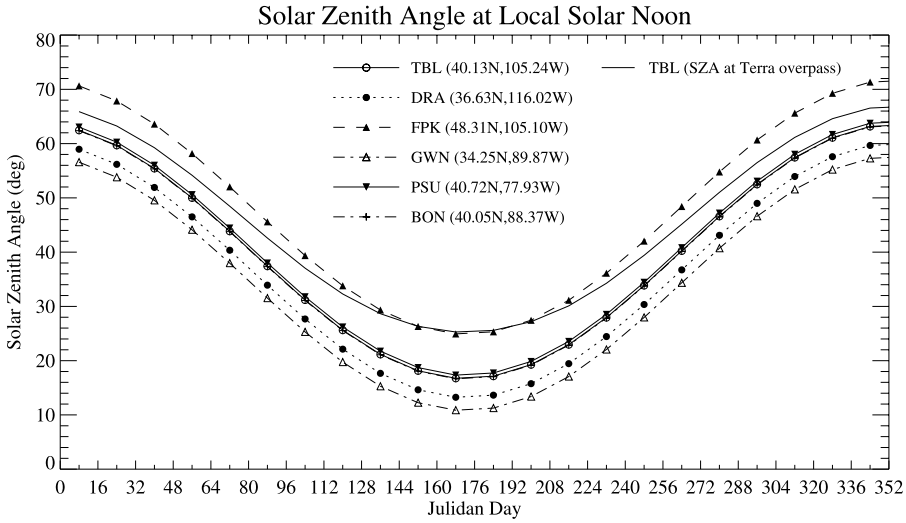

Figure 2. Time series of solar zenith angle at local solar noon over six SURFRAD stations. Solid line without symbols refers to solar zenith angle when EOS-Terra passes over Table Mountain Station.

the area around the stations is sufficiently homogeneous such that the station measurement represents the albedo mean at the MODIS 1-km resolution.

[20] We used here four examples to explore possible spatial scale effects on albedo validation. Two Landsat images, acquired on 15 July and 17 September 2000, cover the Bondville SURFRAD station. For each 1-km by 1-km region collocated with the MODIS pixel, the digital counts were first converted to TOA reflectances and atmospheric correction was then performed with 6S [*Vermote et al.*, 1997b] using the field-measured aerosol optical depths. To obtain the albedo from the Landsat surface directional reflectances, we used the MODIS BRDF parameters to derive the ratio of the hemispherical albedo at local solar noon to the directional surface reflectance at the Landsat near-nadir observing geometry. Finally, narrowband to broadband conversion coefficients [*Liang*, 2000] were applied to derive the Landsat total shortwave albedo.

[21] Over the MODIS 1 km^2 region where the Bondville station is located, the histogram of the Landsat shortwave albedos at the 30-m resolution (Figure 4, upper left panel) shows that the surface albedo is relatively homogeneous (low variance) in July, when vegetation is lush and the Landsat albedo at the field site is only slightly higher by 0.017 than the mean value of the Landsat albedos over the 1 km^2 region. As noted earlier, the MODIS albedo is actually very similar to the field albedo in summer for this station. In September, during the senescent season, the surrounding surface is more heterogeneous as shown by the three modes in the Landsat albedo distribution and the higher overall variance. The Landsat albedo at the field site is higher than the mean value by 0.027 (Figure 4, upper right panel), indicating that a higher bias of 0.027 would be caused when using the albedo of the 30-m by 30-m field around the station to represent the mean albedo value over the MODIS pixel. This explains partly the lower bias of 0.05 for the MODIS 1 km albedo relative to the ground measured albedo in September presented in Figure 1c. As a more appropriate comparison, the MODIS albedos are shown to be similar with the mean values of Landsat albedos over the 1-km by 1-km region.

[22] In Southern Great Plains, the Landsat image acquired on 12 July 2001 covers the sites C01 and E15. There are no corresponding MODIS albedo products in July 2001 due to high frequency of cloud cover in summer over this area. The directional-to-hemispherical conversion is thus not undertaken for these two sites. This, however, does not affect our examination of spatial effect as it has no influence on the distribution of Landsat albedos over the MODIS pixel. Figure 4 (bottom panel) shows that the Landsat shortwave albedo at the site matches well the mean Landsat albedo values over the 1-km by 1-km region, with the difference less than 0.004. This agreement indicates that the field measurements can be directly used to validate the MODIS 1-km albedo products in summer at these two sites. The lower panel of Figure 3 indeed demonstrates the very good agreement between the MODIS albedos and the field measurements.

3.4. Solar Zenith Angle Dependence

[23] An accurate quantification of the solar zenith angle dependence of surface albedo would improve the derivation of daily and monthly mean surface albedo, and increase the accuracy of the modeled shortwave radiation absorbed by the surface. By characterizing the anisotropy of surface reflectivity, the retrieved MODIS BRDF model can be easily integrated to derive the surface albedo under any illumination condition.

[24] We used the MODIS operationally-produced BRDF parameters to derive the surface black sky albedo at various solar zenith angles. The fraction of the direct and diffuse radiation measured in SURFRAD stations are then used to derive the actual surface albedo. We also calculated the average values of ground measured albedos under clear sky conditions over each corresponding 16-day period for various local hours. Figure 5 shows the diurnal cycle of the MODIS (dotted line) and measured (solid line) surface

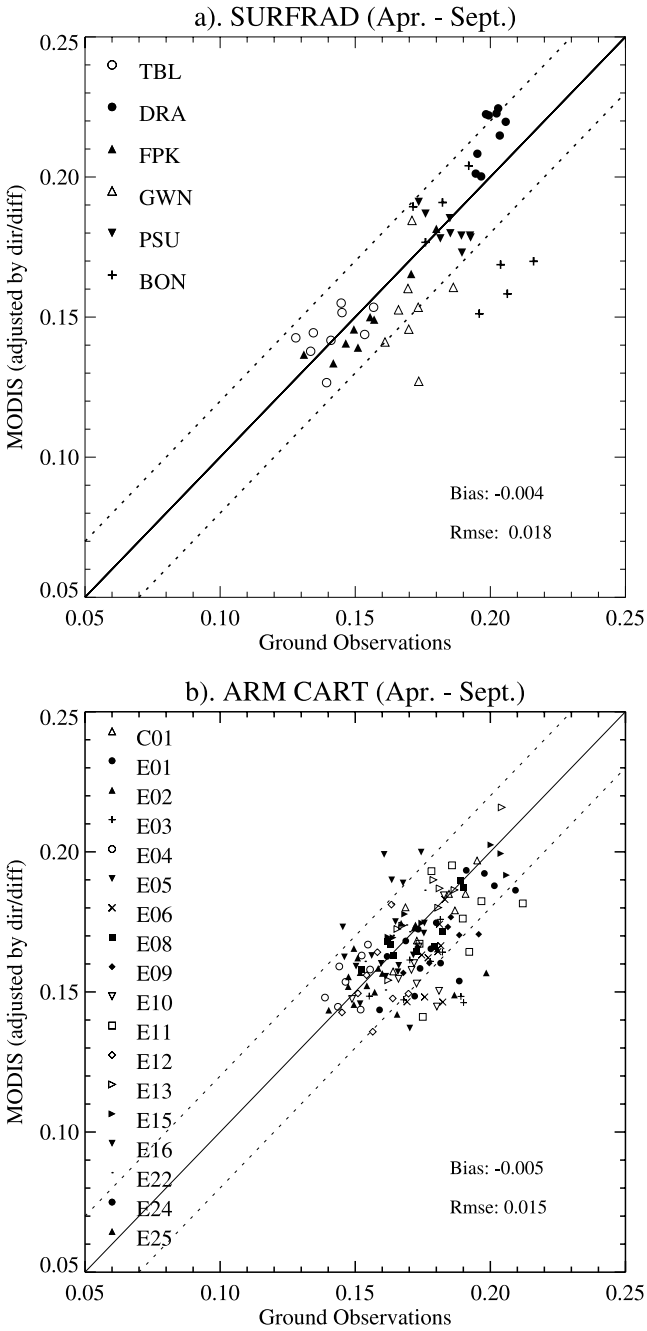

Figure 3. Scatterplots of the MODIS actual shortwave albedo versus the field albedo for the SURFRAD stations (Figure 3a) and CART/SGP sites (Figure 3b) during April–September 2001. All albedos are values at the local solar noon. The dashed lines refer to the boundary of the absolute accuracy requirement of 0.02.

albedos for Fort Peck, Penn State University, and Desert Rock sites during Julian days 208–224 and 240–256, respectively. The field-based measurement reveals that the albedo has the minimum value near noon and increases with the solar zenith angle. The MODIS albedos are shown to capture such a trend. As the solar zenith angle increases, the path lengths of photon interaction with vegetation increases and hence the probability of multiple scattering is increased, leading to higher albedo. For the Fort Peck and Penn State University sites, the MODIS albedos display slightly weaker solar zenith angle dependence than those of the ground measurements.

[25] Also shown in Figure 5 is that largest differences between MODIS and measurements appear when solar zenith angle is greater than 65°. This is mainly due to the decreased accuracy of the RTLSR BRDF model at high solar zenith angles [*Lucht*, 1998]. *Lewis and Barnsley* [1994] also found that an isotropic diffuse approximation may introduce errors in calculating actual albedo from the black sky and white sky albedo when the solar zenith angle is high. The asymmetry of the MODIS actual albedos around local solar noon is caused by the asymmetric fractions of diffuse and direct radiation in the morning and the afternoon as measured over SURFRAD stations.

4. Consistency With CERES TOA Broadband Albedo

4.1. Instrument and Data

[26] Broadband instruments can reduce the narrowband-to-broadband conversion uncertainties in the albedo retrieval compared to the narrowband instruments. The Earth Radiation Budget Experiment (ERBE) is the first multi-satellite system tailored to the measurement of the top-of-atmosphere shortwave, longwave and total radiation fluxes [*Barkstrom*, 1984]. CERES, on board the same Terra platform as MODIS, is a new design based on the successful ERBE scanning radiometer [*Wielicki et al.*, 1996] and is expected to double the ERBE accuracy of radiative fluxes and broadband albedo at the top of the atmosphere. As described in part 1 [*Jin et al.*, 2003], the MODIS surface albedo is retrieved from the TOA spectral radiances through a series of correction and modeling procedures and hence its accuracy depends on each intermediate process. Therefore, it is necessary to check if this downstream product is consistent with an independent measurement of albedo at the top of the atmosphere.

[27] With a field of view of 20-km at nadir, the CERES footprint data has been subsetted from the daily ES-8 files [*Wielicki et al.*, 1996] and pared down to correspond with the 1/2 hour time step of the processed surface data by the CAVE [*Rutan et al.*, 2001]. We used the average of the CERES top-of-atmosphere albedos over all the CERES footprints that fall within a 15-km radius of a given surface site. Only the observations identified as clear scenes in the CAVE data set are used here for our analysis.

4.2. Spatial Analysis of MODIS Albedos Over CERES Footprint

[28] The annual time series of the CERES TOA albedos are also shown in Figures 1a–1c. It should be noted that the CERES TOA albedo is produced for Terra-overpass solar zenith angle while the MODIS albedo is produced at local solar noon. However, the difference between the solar zenith angle at local solar noon and that of Terra overpass (10:30AM) is mostly less than 10 over SURFRAD stations (Figure 2), which does not cause significant albedo change. Considering the different spatial scales of the MODIS albedo and the CERES albedo, it is necessary to check if the albedo for a single MODIS pixel with a 1-km resolution represents the mean status of the albedo over a large region

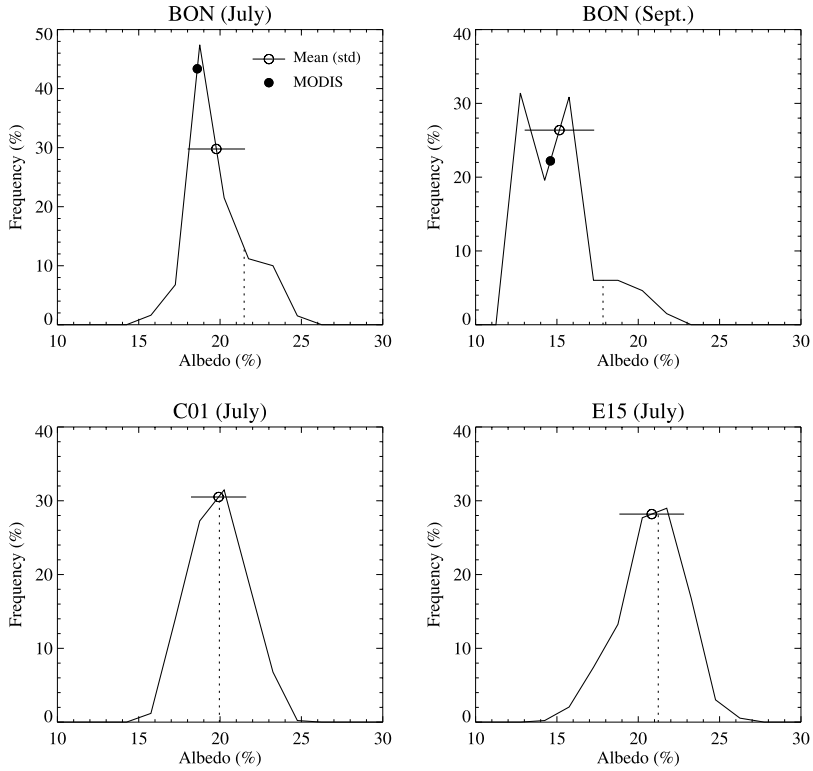

Figure 4. Histograms (solid curve) of surface albedos derived from Landsat ETM+ within a 1-km by 1-km region collocated with the MODIS pixel where the station is located. The mean value and standard deviation of the Landsat albedos within the region are plotted as an open circle and a horizontal line. The Landsat albedo at the actual station location is represented by the dashed line whereas the MODIS albedo at the site is represented by the solid circle. The top panels refer to the Bondville station, and the Landsat imageries were acquired on 15 July and 17 September 2000, respectively. The bottom panels represent the CART sites C01 and E15, and the Landsat imagery was acquired on 12 July 2001.

covered by the CERES average 30-km by 30-km footprint. Figure 6 shows images of the IGBP land cover types and the total shortwave surface albedo from MODIS over a 30-km by 30-km region centered on each SURFRAD station. Note that the albedo images shown are derived for the MODIS observations in May 2001 for the Goodwin Creek station and in early September 2001 for all other SURFRAD stations, which are examples of the full inversion. We also plotted the distribution of the MODIS surface albedos over each 30-km by 30-km region and calculated the regional mean values of the MODIS albedos (Figure 7) for the corresponding time periods.

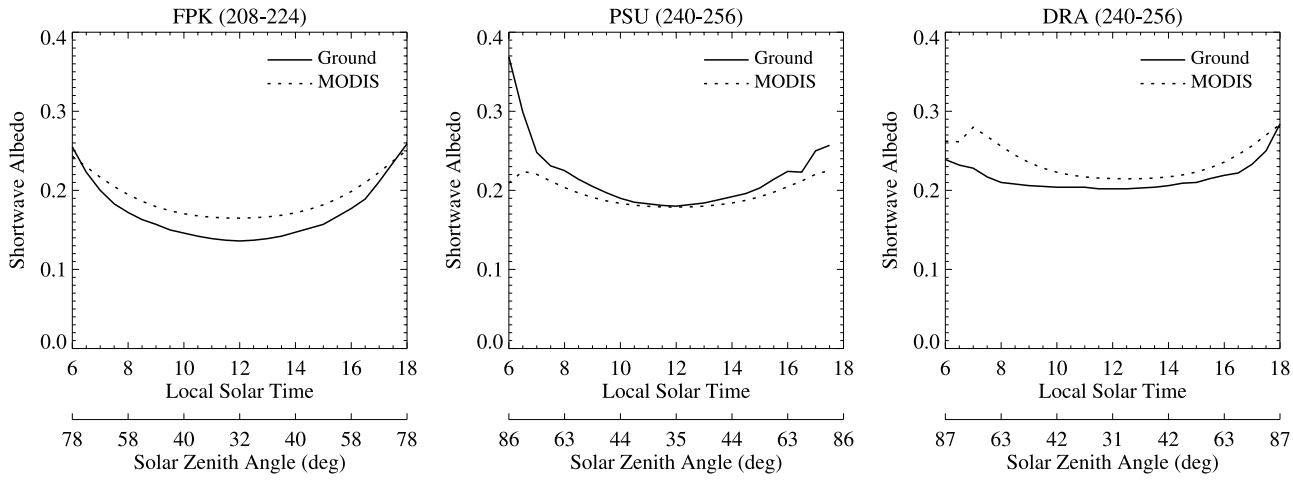

Figure 5. Solar zenith angle dependence of surface albedo as observed from the ground and derived from the retrieved MODIS BRDF model at Fort Peck, Penn State, and Desert Rock SURFRAD stations. The time periods for the observations are also shown in the panel titles.

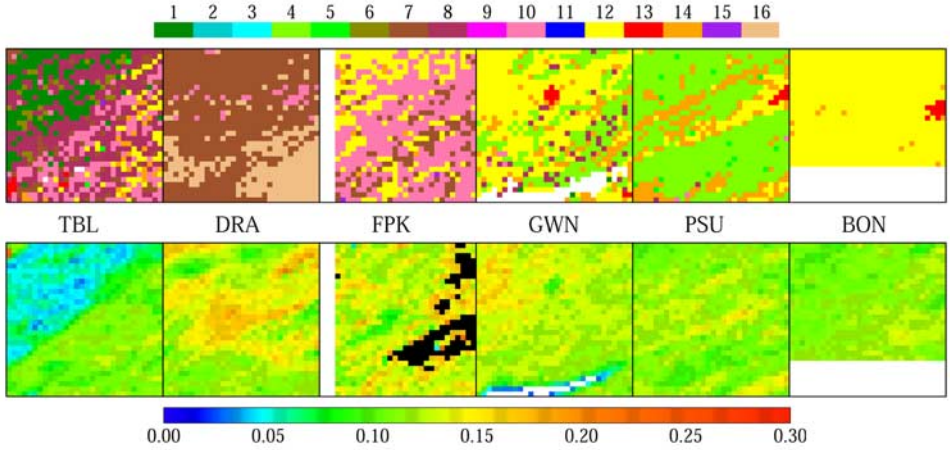

Figure 6. Images of the MODIS IGBP land cover type and the MODIS black sky shortwave albedo over a 30-km by 30-km region centered on each SURFRAD station. Fill values are in black, and white represents water or the pixels outside a tile boundary. IGBP 1. Evergreen needleleaf forests; 3. Deciduous needleleaf forests; 4. Deciduous broadleaf forests; 5. Mixed forests; 6. Closed shrublands; 7. Open shrublands; 8. Woody savannas; 9. Savannas; 10. Grasslands; 12. Croplands; 13. Urban and built-up lands; 14. Cropland/Natural vegetation mosaics; 15. Snow and Ice; 16. Barren.

[29] The albedo histograms show that the Fort Peck, Goodwin Creek, Penn State, and Bondville stations are relatively more homogeneous than the Table Mountain and Desert Rock sites in growing seasons. The extended region around the Fort Peck is covered by grass and crops, and the standard deviation of the MODIS albedos over this region is 0.025. The extended region around the Goodwin Creek station is dominated by croplands with broadleaf forests and woody savannas scattered around. Located in an agricultural area, the Penn State station is surrounded by

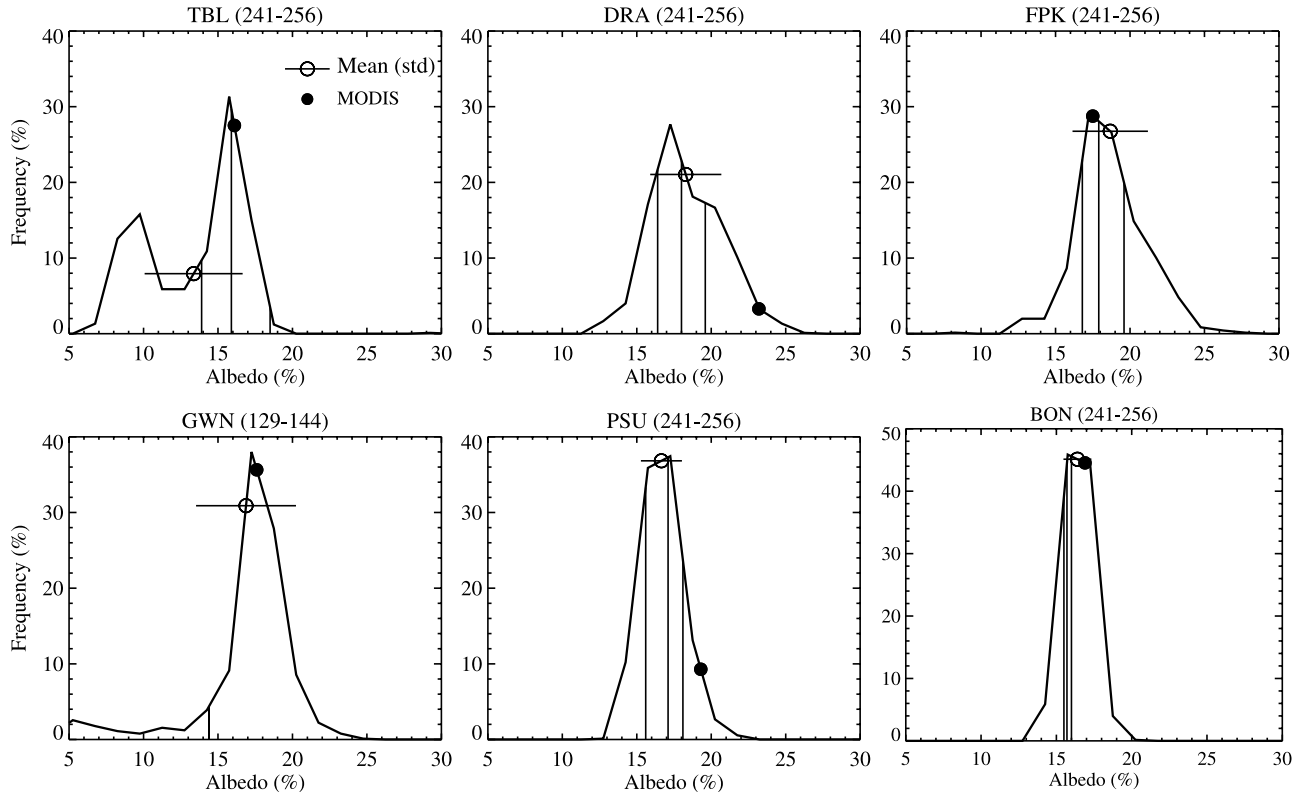

Figure 7. Histograms (solid curve) of the MODIS surface albedos within a 30-km by 30-km region collocated centered in the station. The mean value and standard deviation of the MODIS albedos within the region are plotted as open circle and horizontal line. The MODIS albedo at the actual site is represented by the solid circles whereas the minimum, mean, and maximum of the CERES albedos during the 16-day period are represented by the vertical solid lines from left to right.

broadleaf crops and forests and the MODIS albedos vary by less than 0.014. Croplands dominates the extended region around the Bondville station and the spatial variation of the 1-km albedos is much smaller over the region, although the albedo heterogeneity within a 1-km pixel in September is shown in section 3.3.

[30] For the Table Mountain station, the land cover is needleleaf forests and woody savannas in the northwest, whereas with a mixture of savannas, grasslands, and croplands in the southeast. The two modes of the albedo distribution over the 30-km by 30-km region centered on the Table Mountain station (Figure 7) clearly show the lower albedo value of the forests and higher albedo value of the other vegetation. The Table Mountain station happens to be located in the transitional area and the MODIS albedo at this site has a higher bias of 0.026 compared with the MODIS regional mean.

[31] The land is sparsely vegetated, mainly open shrublands and barren, around the Desert Rock station. Figure 7 shows that the surface albedo is heterogeneous over this region and the MODIS albedo at the site is significantly higher than the MODIS region mean value by 0.049. Correspondingly, a high bias of the MODIS albedo is consistently observed in all seasons (Figure 1a), compared to the CERES TOA albedo. This indicates a significant spatial effect on a direct comparison between the MODIS and CERES albedo around this site.

[32] Figure 7 indicates a very small lower bias of 0.012 for the Fort Peck station and a higher bias of 0.026 for the Penn State station when using the albedo of the MODIS single pixel to represent the regional MODIS mean albedo. Consistent with this scale effect, the time series of MODIS and CERES albedos (Figures 1b and 1c) generally show that the MODIS single pixel albedo is actually lower than the CERES albedo over the Fort Peck station but is higher than the CERES albedo over the Penn State station.

[33] For the Bondville and Goodwin Creek stations, the MODIS albedo of an individual 1-km pixel (denoted by solid circle) was found to represent the MODIS mean value (open circle) over the CERES footprint region quite well, as indicated by Figure 7. Therefore, the MODIS albedo can be directly compared with the CERES TOA albedo for these stations. Correspondingly, Figures 1b and 1c indeed illustrate that the time series of the MODIS station albedos agree well with those of the CERES albedos around these two stations even in the winter season when the MODIS observations do not always relate well to the tower measurements. This tends to confirm our previous suggestion that the winter difference between the MODIS albedo and the ground measurements is most likely the result of the spatial heterogeneity within a 1-km pixel rather than errors in the actual retrievals.

4.3. Consistency Between MODIS Surface Albedo and CERES TOA Albedo

[34] To reduce the spatial effects, we calculated the regional mean of the MODIS albedos over the corresponding CERES footprint for each SURFRAD station. The question now arises whether the surface albedo derived from MODIS observations is consistent with the CERES TOA albedo. Atmospheric aerosols tends to increase the TOA reflectivity in the visible and near infrared bands over

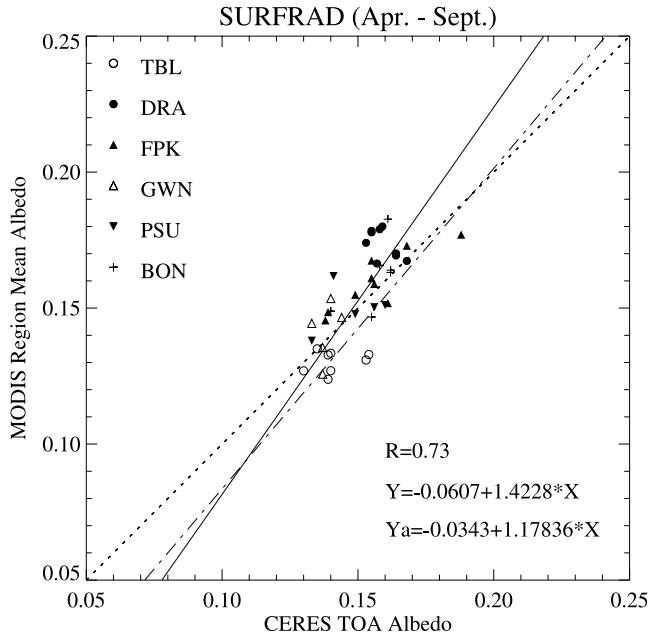

Figure 8. Scatterplots of the MODIS surface black sky albedo, averaged over the 30-km by 30-km region with the station as the center, versus the minimum CERES top-of-the-atmosphere shortwave albedos during the associated 16-day period. The solid line refers to the regression line and the dashed line is 1:1 line. The dot dashed line (Ya) represents the regression against the averaged CERES TOA albedo during the 16-day period.

a relatively dark surfaces [*Rahman*, 1996], and therefore the lowest value of TOA albedos usually represents the clearest cases. For a marginal consistency check, we extracted the minimum CERES albedos during each 16-day period within April–September 2001 for each station to reduce atmospheric effects. Figure 8 shows that the spatially-averaged MODIS albedos are well correlated with the minimum CERES TOA albedos over SURFRAD stations. The solid regression line shows that the CERES TOA albedo is positive when the MODIS surface albedo is zero, indicating the contribution from atmospheric scattering. This reveals the consistency between MODIS surface albedo and CERES TOA albedo. Also note that the 30-km by 30-km region may not exactly match the CERES footprints used for the average in the CAVE data set, which may contribute to part of the difference between the MODIS region mean surface albedo and the CERES TOA albedo.

[35] The regression also shows that the TOA albedo is higher than the surface albedo when the surface albedo is lower than 0.15 but when surface is getting brighter and brighter the TOA albedo is lower than the surface albedo. This agrees with the fact that aerosol reduces the TOA reflectivity over relatively bright land targets [*Rahman*, 1996]. As expected, the breakpoint increases to 0.2 when the CERES TOA albedos averaged over each 16-day period are instead used for the regression, which apparently contains more atmospheric effects. A radiative transfer-based simulation is necessary in the future to further investigate the consistency between MODIS surface albedo and CERES TOA albedo given very accurate atmospheric

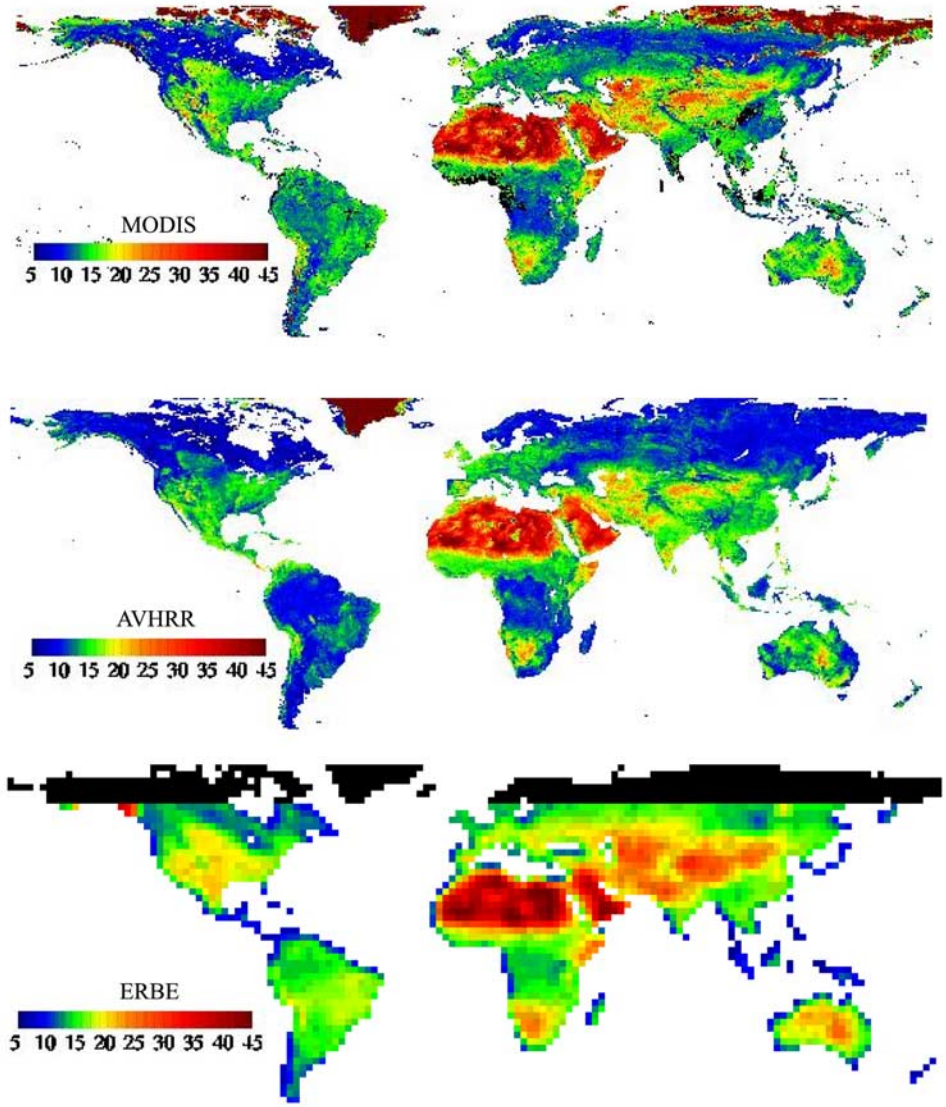

Figure 9. Global September albedo from the MODIS operational product with 1-km resolution, the AVHRR observations with 0.15° resolution [*Csiszar and Gutman*, 1999], and the ERBE observations with 2.5° resolution [*Li and Garand*, 1994]. Fill values are in black.

information such as aerosol optical depth and amount of water vapor.

5. Comparison With Other Global Albedo Data Sets

[36] A number of algorithms were developed to retrieve regional or global surface albedo from various satellite instruments [*Pinker and Laszlo*, 1992; *Li and Garand*, 1994; *Weiss et al.*, 1999; *Gutman*, 1999; *Csiszar and Gutman*, 1999; *Pinty et al.*, 2000a, 2000b]. *Li and Garand* [1994] produced a monthly surface broadband albedo climatology with a 2.5° resolution using five years of ERBE clear-sky data during 1985-1989. The TOA broadband albedo was first derived with ERBE Angular Distribution Models and a linear parameterization was then established to derive surface albedo directly from the TOA albedo assuming a fixed aerosol optical depth of 0.05 at 550 nm. A higher resolution albedo product was derived from weekly composites of NOAA AVHRR/GAC GVI data sets, which contains the 5-year monthly means of surface broadband shortwave albedos at a 0.15° spatial resolution under clear-sky and snow-free conditions during 1985–1991 [*Csiszar and Gutman*, 1999]. In Csiszar and Gutman's retrieval algorithm, a narrow-to-broadband conversion was first performed and angular and atmospheric corrections similar to Li and Garand's methods were undertaken. Furthermore, albedo is normalized to overhead sun illumination conditions. Both ERBE and AVHRR albedo products were validated with available field measurements [*Li and Garand*, 1994; *Csiszar and Gutman*, 1999]. To examine the consistency between the MODIS albedos and the above two historical data sets which are commonly used by climate modelers, we aggregated the MODIS albedos in June and September 2001 from 1-km resolution to 0.15° and 2.5° resolution for comparison.

[37] Figure 9 shows the operational MODIS 1-km surface black sky albedo at local solar noon, the 0.15° AVHRR

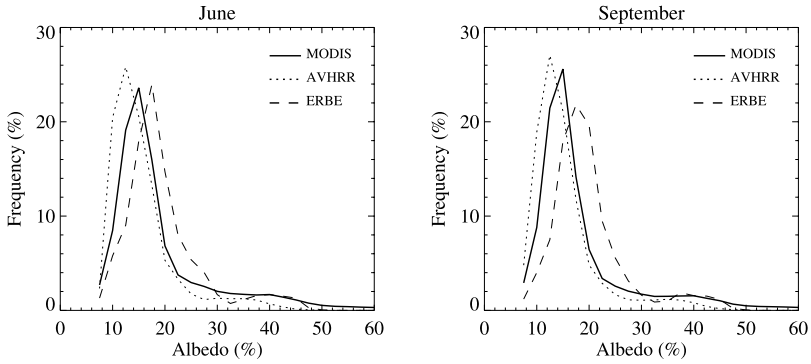

Figure 10. Histograms of global surface albedos at 2.5° resolution.

albedo under overhead sun conditions, and the 2.5° ERBE monthly mean surface albedo in September. Similar spatial patterns of surface albedo are apparent in both the MODIS and AVHRR data sets. The surface albedo of boreal forest is as low as 0.1 while the albedo of desert is around 0.35. The intermediate albedo values appear in grasslands and savannas. This coarse scale pattern is also observed in the ERBE low-resolution albedo product. The fine resolution MODIS albedos, however, capture the most detailed spatial features. In general, global albedo distributions of these three data sets are similar in June and September as shown by the histograms in Figure 10, but some systematic biases exist. Figure 11 shows that the latitude distribution of surface albedos are also similar. The maximum albedo, for example, occurs around 20°N, where the largest area of desert is located.

[38] Figure 12 shows that the MODIS black sky albedo agrees well with the AVHRR albedo. The RMSE is 0.025. The MODIS albedo has a slightly high bias of 0.016. Note that the albedo under off-nadir direct illumination at local solar noon is usually higher than when the sun is overhead. Significantly higher MODIS albedos are found in relatively bright areas such as Central Asia and Northern Africa, as shown in Figure 9. Over these areas, the aerosol optical depth is higher than the prescribed 0.05 at 550nm [*Torres et al.*, 2002]. Aerosols are found to reduce the albedo of relative bright targets [*Rahman*, 1996], and therefore the possible residual aerosol effect may also contribute to the lower surface albedo derived from the AVHRR observations [*Csiszar and Gutman*, 1999] over these bright areas.

[39] The MODIS albedo is also generally higher than that of AVHRR in South America, especially on the eastern side of the continent. Over this region, various studies have shown that 100 million hectares of land have been degraded as a result of deforestation and some 70 million hectares of land have been overgrazed during late 80's and early 90's [*United Nations Environment Programme*, 2000]. This continuing land cover change may cause some of the increase in surface albedo from historical observations to more recent MODIS observations. In addition to deforestation, there is very intense biomass burning in the Amazon basin. Residual contamination from smoke may also contribute to the differences in the albedo products.

[40] The correlation between the MODIS and ERBE albedo is 0.90 and the RMSE is 0.047. On the average, the ERBE albedo has a higher bias of 0.034 compared to the MODIS albedo. The ERBE data set is a daily mean albedo and is expected to be higher than those under an overhead illumination and at local solar noon. Moreover, cloud identification is more difficult for the ERBE observations at coarse resolution, leading to an increase in the retrieved albedo.

[41] The differences between the MODIS albedo and those derived from the historical AVHRR and ERBE observations are in the range of the uncertainties attributed to the diversity of the instruments, the retrieval algorithms, the angular geometry, and environmental change, such as deforestation. The operational MODIS albedo is thus considered to be comparable with the historical AVHRR and ERBE albedo data sets.

6. Discussion and Conclusions

[42] Surface reflectivity varies with time and space. Retrieving surface albedo from space relies on prerequisite

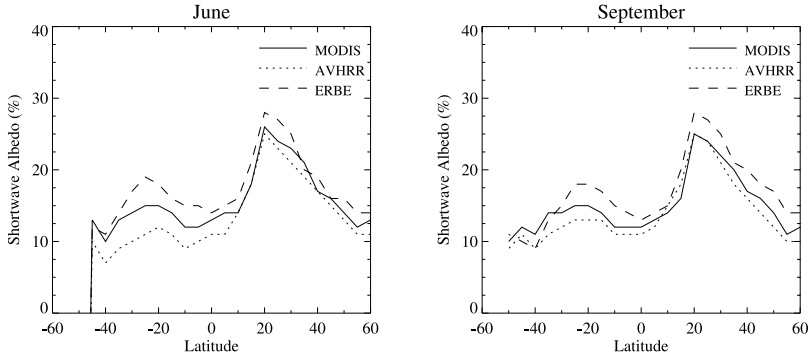

Figure 11. Zonal means of surface albedo in June and September.

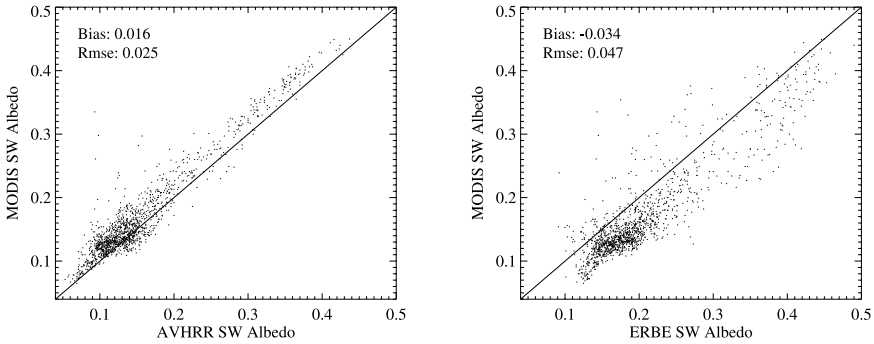

Figure 12. Scatterplot of the MODIS albedo versus the AVHRR Albedo aggregated to 2.5° resolution and that of the MODIS albedo versus the ERBE albedo at 2.5° resolution.

atmospheric information in addition to narrowband-to-broadband conversion and directional-to-hemispherical conversion. No single test can ever sufficiently demonstrate the uncertainty of the operational surface albedo product derived from satellite observations. A hierarchical framework is therefore necessary with many validation tiers being performed at different stages [*Justice et al.*, 2000]. The existing radiation networks such as SURFRAD have long term ground measurements and cover relatively diverse land cover types [*Augustine et al.*, 2000]. A comparison with these ground measurements provides a preliminary validation of surface albedo product and helps to identify possible situations where the satellite product has larger uncertainty. The quantification of errors from each source, however, is impossible without a closure field campaign involving ground, aircraft, and satellite measurements at different spatial scales. Both established network and field campaign is limited by spatial coverage, and hence an intercomparison with other global albedo products is also necessary.

[43] We examined the accuracy of the MODIS albedo products using two sets of coincident field measurements. During April–September 2001, the MODIS surface albedo generally met the absolute accuracy requirement of 0.02 for six diverse SURFRAD stations and eighteen sites in the CART/SGP area. In both networks, the root mean square errors are less than 0.0177 and a relatively minor lower bias of 0.004 was observed for the MODIS albedo products. The MODIS BRDF model also captures the solar zenith angle dependence of the surface albedo as indicated in field measurements. For the Bondville station and two CART/SGP sites, a spatial analysis of the albedos at a 30-m resolution derived from Landsat ETM+ observations in July reveals that the albedo at the field site represents well the mean albedo value over the collocated MODIS 1-km by 1-km region and thus the validation with the field measurements is appropriate over the study stations in summer. The increased heterogeneity in fall partially explains the discrepancy between the MODIS albedos and field values in fall. Further studies are needed to explain the observed discrepancies in winter over these sites.

[44] We also investigated the consistency between the MODIS surface albedos and the contemporary CERES TOA albedos and found that the MODIS surface shortwave albedos, derived from spectral albedos, are consistent with contemporary and collocated CERES TOA albedos derived directly from broadband observations. The MODIS albedo is also comparable to commonly used surface albedo data sets derived from the historical AVHRR and ERBE observations [*Csiszar and Gutman*, 1999; *Li and Garand*, 1994], with RMSE values of 0.025 and 0.047, respectively.

[45] This study is a preliminary validation of the MODIS albedo product. We intend to continue the validation as more data from ground measurements and field campaigns are available [*Schaaf et al.*, 2002; *Liang et al.*, 2002]. Note that the MODIS albedos are produced for seven spectral bands and three broadbands, which offers more precision in the spectral characteristics of surface albedo. With a 1-km resolution, the MODIS albedo can capture considerable spatial variability of surface reflectivity and thus helps to improve the albedo representation in climate models [*Tsvetsinskaya et al.*, 2002; *Jin et al.*, 2002]. The 16-day temporal resolution of the MODIS albedo product also provides a great opportunity to monitor and identify human-induced albedo change [*Intergovernmental Panel on Climate Change* (*IPCC*), 2001].

[46] **Acknowledgments.** Surface radiometric observations came from the CERES/ARM Validation Experiment (CAVE) and are available on the world wide web at http://www-cave.larc.nasa.gov/cave/. We thank all field participants who made measurements over the SURFRAD and CART/SGP network stations. This work was supported by NASA's MODIS project under contract NAS5-31369. W.L. was supported by the German Ministry of Education and Research in the DEKLIM Programme.

References

Augustine, J. A., J. DeLuisi, and C. Long, SURFRAD: A national surface radiation budget network for atmospheric research, *Bull. Am. Meteorol. Soc.*, *81*, 2341–2357, 2000.

Barkstrom, B. R., The Earth Radiation Budget Experiment (ERBE), *Bull. Am. Meteorol. Soc.*, *65*, 1170–1185, 1984.

Bonan, G. B., A land surface model (LSM version 1.0) for ecological, hydrological, and atmospheric studies: Technical description and user's guide, *NCAR Tech. Note NCAR/TN-147 + STR*, Natl. Cent. for Atmos. Res., Boulder, Colo., 1996.

Collins, J. B., and C. Woodcock, Combining geostatistical methods and hierarchical scene models for analysis of multiscale variation in spatial data, *Geogr. Anal.*, *32*, 48–63, 2000.

Csiszar, I., and G. Gutman, Mapping global land surface albedo from NOAA AVHRR, *J. Geophys. Res.*, *104*, 6215–6228, 1999.

DeLuisi, J. J., J. A. Augustine, C. R. Cornwall, G. B. Hodges, C. N. Long, and D. L. Wellman, NOAA's SURFRAD: Surface radiation measurements at six regional stations, paper presented at 10th Conference on Atmospheric Radiation Measurements, Natl. Oceanic and Atmos. Admin., Madison, Wisc., 1999.

Dickinson, R. E., Land processes in climate models, *Remote Sens. Environ.*, *51*, 27–38, 1995.

Dickinson, R. E., A. Henderson-Sellers, and P. J. Kennedy, Biosphere-Atmosphere Transfer Scheme (BATS) Version 1e as coupled to the NCAR community model, *NCAR Tech. Note NCAR/TN-387 + STR*, Natl. Cent. for Atmos. Res., Boulder, Colo., 1993.

Gutman, G. G., On the use of long-term global data of land reflectances and vegetation indices derived from the advanced very high resolution radiometer, *J. Geophys. Res.*, *104*, 6241–6255, 1999.

Hansen, J. E., Efficient three dimensional global models for climate studies: Models I and II, *Mon. Weather Rev.*, *11*, 609–662, 1983.

Henderson-Sellers, A., and M. F. Wilson, Surface albedo data for climatic modeling, *Rev. Geophys.*, *21*, 1743–1778, 1983.

Intergovernmental Panel on Climate Change (IPCC), *Climate Change 2001: The Scientific Basis*, Cambridge Univ. Press, New York, 2001.

Jin, Y., C. B. Schaaf, F. Gao, X. Li, A. H. Strahler, X. Zeng, and R. E. Dickinson, How does snow impact the albedo of vegetated land surfaces as analyzed with MODIS data?, *Geophys. Res. Lett.*, *29*(10), 1374, 10.1029/2001GL014132, 2002.

Jin, Y., C. B. Schaaf, F. Gao, X. Li, A. H. Strahler, W. Lucht, and S. Liang, Consistency of MODIS surface bidirectional reflectance distribution function and albedo retrievals: 1. Algorithm performance, *J. Geophys. Res.*, *108*, doi:10.1029/2002JD002803, in press, 2003.

Justice, C. O., A. Belward, J. Morisette, J. L. Privette, and F. Baret, Developments in the validation of satellite products for the study of land surface, *Int. J. Remote Sens.*, *21*, 3383–3390, 2000.

Lewis, P., and M. J. Barnsley, Influence of the sky radiance distribution on various formulations of the Earth surface albedo, paper presented at International Symposium on Physical Measurements and Signatures in Remote Sensing, Int. Sco. for Photogramm. and Remote Sens., Val d'Isere, France, 1994.

Li, Z., and L. Garand, Estimation of surface albedo from space: A parameterization for global application, *J. Geophys. Res.*, *99*, 8335–8350, 1994.

Liang, S., Narrowband to broadband conversions of land surface albedo, I, Algorithms, *Remote Sens. Environ.*, *76*, 213–238, 2000.

Liang, S., A. H. Strahler, and C. W. Walthall, Retrieval of land surface albedo from satellite observations: A simulation study, *J. Appl. Meteorol.*, *38*, 712–725, 1999.

Liang, S., H. Fang, M. Chen, C. J. Shuey, C. Walthall, C. Daughtry, J. Morisette, C. Schaaf, and A. Strahler, Validating MODIS land surface reflectance and albedo products: Methods and preliminary results, *Remote Sens. Environ.*, *83*, 149–162, 2002.

Long, C. N., and T. P. Ackerman, Identification of clear skies from broadband pyranometer measurements and calculation of downwelling shortwave cloud effects, *J. Geophy. Res.*, *105*, 15,609–15,626, 2000.

Lucht, W., Expected retrieval accuracies of bidirectional reflectance and albedo from EOS-MODIS and MISR angular sampling, *J. Geophys. Res.*, *103*, 8763–8778, 1998.

Lucht, W., C. B. Schaaf, and A. H. Strahler, An algorithm for the retrieval of albedo from space using semiempirical BRDF models, *IEEE Trans. Geosci. Remote Sens.*, *38*, 977–998, 2000a.

Lucht, W., A. H. Hyman, A. H. Strahler, M. J. Barnsley, P. Hobson, and J.-P. Muller, A comparison of satellite-derived spectral albedos to ground-based broadband albedo measurements modeled to satellite spatial scale for a semidesert landscape, *Remote Sens. Environ.*, *74*, 85–98, 2000b.

Pinker, R., and I. Laszlo, Modeling surface solar irradiance for satellite applications on a global scale, *J. Appl. Meteorol.*, *31*, 194–211, 1992.

Pinker, R. T., I. Laszlo, Y. Wang, and J. D. Tarpley, GCIP GOES shortwave radiation budgets: Validation activity, paper presented at Second International Scientific Conference on the Global Energy and Water Cycle, World Clim. Res. Program, Washington, D. C., 1996.

Pinty, B., F. Roveda, M. M. Verstraete, N. Gobron, Y. Govaerts, J. V. Martonchik, D. J. Diner, and R. A. Kahn, Surface albedo retrieval from Meteosat, 1, Theory, *J. Geophy. Res.*, *105*, 18,099–18,112, 2000a.

Pinty, B., F. Roveda, M. M. Verstraete, N. Gobron, Y. Govaerts, J. V. Martonchik, D. J. Diner, and R. A. Kahn, Surface albedo retrieval from Meteosat, 2, Applications, *J. Geophy. Res.*, *105*, 18,113–18,134, 2000b.

Rahman, H., Atmospheric optical depth and water vapor effects on the angular characteristics of surface reflectance in NOAA AVHRR, *Int. J. Remote Sens.*, *17*, 2981–2999, 1996.

Rodgers, C. D., *Inverse Methods for Atmospheric Sounding: Theory and Practice*, World Sci., River Edge, N. J., 2000.

Rutan, D. A., F. G. Rose, N. Smith, and T. P. Charlock, Validation data set for CERES Surface and Atmospheric Radiation Budget (SARB), *GEWEX News*, *11*(1), 11–12, 2001.

Schaaf, C. B., et al., First operational BRDF, albedo and nadir reflectance products from MODIS, *Remote Sens. Environ.*, *83*, 135–148, 2002.

Sellers, P. J., Remote sensing of the land surface for studies of global change, NASA/GSFC International Satellite Land Surface Climatology Project report, NASA Goddard Flight Space Cent., Greenbelt, Md., 1993.

Sellers, P. J., D. A. Randall, G. J. Collatz, J. A. Berry, C. B. Field, D. A. Dazlich, C. Zhang, G. D. Collelo, and L. Bounoua, A revised land surface parameterization (SiB2) for atmospheric GCMs, part I, Model formulation, *J. Clim.*, *9*, 676–705, 1996.

Stokes, G. M., and S. E. Schwartz, The Atmospheric Radiation Measurement (ARM) program: Programmatic background and design of the cloud and radiation test bed, *Bull. Am. Meteorol. Soc.*, *75*, 1201–1221, 1994.

Strahler, A. H., W. Wanner, C. B. Schaaf, X. Li, B. Hu, J.-P. Muller, P. Lewis, and M. J. Barnsley, MODIS BRDF/Albedo product: Algorithm theoretical basis document, *NASA EOS-MODIS Doc.*, *Version 4.0*, pp. 9–17, Natl. Aeronau. and Space Admin., Washington, D. C., 1996.

Strugnell, N. C., and W. Lucht, An algorithm to infer continental-scale albedo from AVHRR data, land cover class, and field observations of typical BRDFs, *J. Clim.*, *14*, 1360–1376, 2001.

Tian, Y., et al., Multiscale analysis and validation of the MODIS LAI product over Maun, Botswana, I, Uncertainty assessment, *Remote Sens. Environ.*, *83*, 414–430, 2002.

Torres, O., P. K. Bhartia, J. R. Herman, A. Sinyuk, and B. Holben, A long term record of aerosol optical thickness from TOMS observations and comparison to AERONET measurements, *J. Atmos. Sci.*, *59*, 398–413, 2002.

Trenberth, K. E., *Climate System Modeling*, Cambridge Univ. Press, New York, 1992.

Tsvetsinskaya, E. A., C. B. Schaaf, F. Gao, A. H. Strahler, R. E. D. X. Zeng, and W. Lucht, Relating MODIS-derived surface albedo to soils and rock types over northern Africa and the Arabian Peninsula, *Geophys. Res. Lett.*, *29*(9), 1353, doi:10.1029/2001GL014096, 2002.

United Nations Environment Programme, *Global Environment Outlook*, Oxford Univ. Press, New York, 2000.

Vermote, E. F., N. Z. Saleous, C. O. Justice, Y. J. Kaufman, J. Privette, L. Remer, J. C. Roger, and D. Tarne, Atmospheric correction of visible to middle infrared EOS-MODIS data over land surface, background, operational algorithm and validation, *J. Geophys. Res.*, *102*, 17,131–17,141, 1997a.

Vermote, E. F., D. Tanré, J. L. Deuzé, M. Herman, and J. J. Morcette, Second simulation of the satellite signal in the solar spectrum: An overview, *IEEE Trans. Geosci. Remote Sens.*, *35*, 675–686, 1997b.

Wanner, W., A. H. Strahler, B. Hu, P. Lewis, J.-P. Muller, X. Li, C. B. Schaaf, and M. J. Barnsley, Global retrieval of bidirectional reflectance and albedo over land from EOS MODIS and MISR data: Theory and algorithm, *J. Geophys. Res.*, *102*, 17,143–17,162, 1997.

Weiss, M., F. Baret, M. Leroy, A. Begue, O. Hautecoeur, and R. Santer, Hemispherical reflectance and albedo estimates from the accumulation of across-track Sun-synchronous satellite data, *J. Geophys. Res.*, *104*, 22,221–22,232, 1999.

Wielicki, B. A., B. R. Barkstrom, E. F. Harrison, G. L. S. R. B. Lee, and J. E. Cooper, Clouds and the Earth's Radiant Energy System (CERES): An Earth Observing System experiment, *Bull. Am. Meteorol. Soc.*, *77*, 853–868, 1996.

Wielicki, B. A., et al., Clouds and the Earth's Radiant Energy System (CERES): Algorithm overview, *IEEE Trans. Geosci. Remote Sens.*, *36*, 1127–1140, 1998.

Woodcock, C., and V. Harward, Nested-hierarchical scene models and image segmentation, *Int. J. Remote Sens.*, *13*, 3167–3187, 1992.

F. Gao, Y. Jin, X. Li, C. B. Schaaf, A. H. Strahler, and C. E. Woodcock, Department of Geography and Center for Remote Sensing, Boston University, Boston, MA 02215, USA. (yfj@bu.edu; fgao@crsa.bu.edu; lix@crsa.bu.edu; schaaf@crsa.bu.edu; alan@bu.edu; curtis@bu.edu)

S. Liang, Department of Geography, 2181 LeFrak Hall, College Park, MD 20742, USA. (sliang@geog.umd.edu)

W. Lucht, Potsdam-Institut für Klimafolgenforschung (PIK), Telegrafenberg C4, Postfach 60 12 03, D14412 Potsdam, Germany. (wolfgang.lucht@pik-potsdam.de)